Entangled-Photon Imaging of a Pure Phase Object

Ayman F. Abouraddy,* Patrick R. Stone, Alexander V. Sergienko, Bahaa E. A. Saleh, and Malvin C. Teich
Quantum Imaging Laboratory,† Departments of Electrical & Computer Engineering and Physics, Boston University, Boston, Massachusetts 02215-2421, USA
(Received 22 November 2003; published 17 November 2004)

We demonstrate experimentally and theoretically that a coherent image of a pure phase object [implemented by a microelectromechanical system (MEMS) micromirror array] may be obtained by use of a spatially *incoherent* illumination beam. This is accomplished by employing a two-beam source of entangled photons generated by spontaneous parametric down-conversion. One of the beams probes the phase object while the other is scanned. Though each of the beams is, in and of itself, spatially incoherent, the pair of beams exhibits higher-order interbeam coherence.

DOI: 10.1103/PhysRevLett.93.213903 PACS numbers: 42.65.Lm, 03.65.Ud, 03.67.Mn

Introduction.—We demonstrate that the imaging of a phase object can be achieved by making use of a special nonthermal light source that is incoherent in second order but exhibits higher-order coherence properties, *viz.* a source of twin-beam light emitted by spontaneous parametric down-conversion (SPDC) in a nonlinear optical crystal [1]. Each of the emitted beams lacks second-order spatial coherence (as well as temporal coherence), but the two beams are endowed with interbeam higher-order spatial (and temporal) coherence, which is exhibited via enhanced photon coincidences (bunching) along directions where photon momentum is conserved [2–7]. Such sources exhibit unique quantum-correlation features that have generated considerable interest in the context of imaging, particularly in the past few years [8–15]. Since the photons are emitted in pairs, in an entangled quantum state, imaging using such a light source has been referred to as *entangled-photon imaging*. The class of objects that has heretofore been examined in this context has been limited to that of amplitude objects [8,9], *viz.* objects with a spatially varying amplitude transmittance. Such objects have usually been amplitude-modulating transparencies inserted in a transmission configuration.

The higher-order coherence properties of classical light have, of course, long been used for imaging, most notably in the Hanbury-Brown–Twiss (HBT) interferometer [16]. Amplitude as well as phase imaging is possible, by making use of multiple beams and multiple detectors [17]. The principal disadvantage of such imaging systems is the fact that the information-bearing signal is buried in a strong background; it is essentially washed out when the area and response time of the detector are substantially greater than the coherence area and coherence time of the source, respectively, as is often the case. In the imaging configuration considered here, photon coincidences are measured in much the same way as they are in the HBT interferometer, but the deleterious strong background term is absent.

Our system is constructed in a so-called *ghost-imaging* configuration, in which only one of the beams interacts with the object. The duality between partial coherence and partial entanglement [18] assures us that an analogous ghost-imaging system can be constructed using thermal light and, indeed, the implementation of such a system has recently been suggested [19]. The principal challenge is finding means to suppress the strong background. One way of achieving this is to drastically reduce the number of temporal and spatial modes associated with the thermal light. Magatti *et al.* [20] have used pseudothermal light and a spatial pinhole to do so. The pseudothermal light provides a long coherence time [21], whereas the pinhole provides a large coherence area [22]. This configuration thus effectively endows the thermal light with second-order, as well as fourth-order, coherence so that it can be used to image phase objects according to the standard prescription [22]. It is therefore distinct from the configuration studied in the present work, in which the spatial distribution of a pure phase object is measured using an optical field that lacks second-order spatial coherence but is endowed with higher-order spatial coherence. It has been shown that such a two-photon imaging system (*viz.* a system that makes use of optical beams in a two-photon quantum state) requires the presence of entanglement to function as a coherent imaging system (i.e., as a system that is capable of imaging a phase object) [10].

We proceed to provide an experimental demonstration of entangled-photon imaging of a *pure phase object* in a *reflection* configuration. The phase object is illuminated by one of the (spatially incoherent) beams and the photon-coincidence rate for detectors placed in both beams is measured. This allows the formation of a coherent image of the phase object. Phase objects are of special interest in quantum information processing since they introduce a unitary operation that is reversible (in contrast to amplitude masks of any form).

Imaging configuration.—The arrangement used in our experiment is shown schematically in Fig. 1. The source of light is spontaneous parametric down-conversion generated in a nonlinear crystal (NLC) pumped by a laser beam (LASER). The down-converted photons are emitted in pairs in a collinear configuration; they are subse-

 © 2004 The American Physical Society

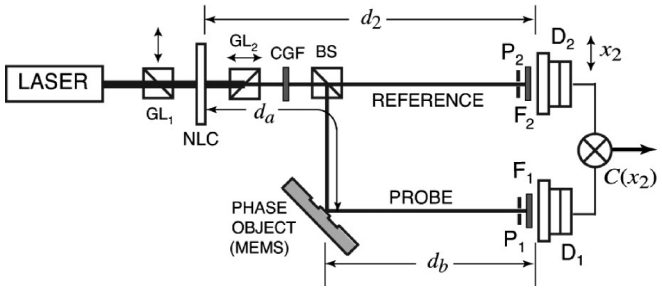

FIG. 1. Experimental arrangement for the quantum imaging of a reflective pure phase object (MEMS). NLC represents the nonlinear crystal, CGF stands for a colored glass filter, GL_1 and GL_2 are two orthogonally oriented Glan-Laser polarizing beam splitters, BS is a nonpolarizing beam splitter, P_1 and P_2 are vertical slits, F_1 and F_2 are interference filters, D_1 and D_2 are single-photon detectors, and ⊗ represents an electronic coincidence circuit.

quently separated into two beams (each of which is spatially incoherent, as indicated above). One of the beams (PROBE) impinges on the object, in our case a microelectromechanical system (MEMS) micromirror array configured so as to modulate the phase of the impinging wave front. Upon reflection from the object, the probe beam is detected by a single detector D_1 fitted with a fixed small pinhole P_1. The other beam (REFERENCE) does not interact with the object, and is simply directed to a small pinhole P_2 and a detector D_2. The terms "PROBE" and "REFERENCE" are used since they are more descriptive in this case than the usual terminology: signal and idler. The coincidence rate $C(x_2)$ of the photons detected by the two detectors is measured as detector D_2 (together with pinhole P_2) is scanned while P_1 is held fixed. As will be shown theoretically, and confirmed experimentally, if the intervening optical system is appropriately designed, a coherent image of the phase object may be obtained.

The system is configured such that the probe beam cannot, by itself, generate an image of the phase object. First, detector D_1 is a single fixed detector lacking spatial resolution. Second, the probe beam lacks second-order spatial coherence. Third, the distance d_b between the object and the detector D_1 is deliberately chosen such that D_1 does not lie in the far field (Fresnel number $N_F \approx 2.02$), thus precluding the formation of a far-field diffraction pattern of the phase object that could provide information about the phase spatial distribution, were the beam coherent.

The pure phase object we consider is characterized by a spatially varying unimodular complex amplitude transmittance or reflectance of the form $\exp[i\theta(\mathbf{r})]$, where $\theta(\mathbf{r})$ is a real function of the position $\mathbf{r}$ in the object plane. Such an object could not be imaged directly by using a conventional single-lens imaging system satisfying the imaging condition and a conventional intensity-sensitive detector. Since such a system ideally provides a geometric mapping between each point in the object plane and a corresponding point in the image plane, it yields no phase information. In the context of entangled-photon imaging, such a system was implemented in Ref. [8] for imaging the intensity transmittance of an object.

In conventional coherent optics, a phase object is typically imaged either interferometrically or by using an optical spatial Fourier-transform system, which converts the phase distribution of the optical wave front at the object plane into a spatially varying amplitude distribution that is detectable by an intensity-sensitive detector. Two examples of Fourier-transform systems are (1) a single-lens 2-f system, and (2) free-space propagation in the Fraunhofer regime, commonly known as the far field [23]. In our entangled-photon imaging system, we have effectively implemented a Fourier-transform configuration based on lensless propagation to the far field, a system similar to that used in Ref. [24]. The exact Fourier transform is achieved only in the Fraunhofer-diffraction region, which necessitates traveling a prohibitively long distance [23]. The distances used in our experiment actually place the image at a location $d = d_a + d_2$ (Fresnel number $N_F \approx 0.78$), which is intermediate between Fresnel and Fraunhofer diffraction.

Theory.—A theoretical expression for the photon-coincidence rate in the above imaging configuration is obtained by using the formalism developed in Ref. [18]. The advanced-wave interpretation, pioneered by D. N. Klyshko [25], provides a rationale for the formation of an approximate Fraunhofer pattern of the phase object.

In view of the advanced-wave interpretation, the image obtained by scanning the coincidence rate $C(x_2)$ is the same as that obtained when a point source at P_1 illuminates the phase object, and the diffraction pattern is obtained at a distance. The finite size of P_1 introduces partial coherence into the imaging system; if sufficiently large it renders the system effectively incoherent [18]. The size of the pinhole P_2, on the other hand, sets a limit on the resolution of the scanned coherent image.

To simplify the calculation we assume that the nonlinear crystal is thin ($l \rightarrow 0$) and that the pump is a plane wave normally incident on the crystal. This zeroth-order approximation overestimates the width of the far-field image produced, since a broad spatial spectrum is implicit in the thin-crystal approximation. We have therefore approximately accommodated the finite width of the pump and finite crystal thickness by multiplying the calculated value of $C(x_2)$ by the measured conventional far-field image of the reference obtained from the single-photon rates at D_2, which is independent of the object and depends only on the parameters of the pump beam and the nonlinear crystal.

Experiment.—The pure phase object used in our experiments comprised a 12×12 array of gold-plated micromirrors, each of dimension 300×300 μm. The overall size of the object was therefore 3.6×3.6 mm. The object was fully illuminated by the down-converted

beam, which has a broad angular spectrum. The height of each mirror, with respect to a fixed datum, is altered via an electrostatic potential. If one micromirror is pulled down from the datum a distance Δ, the portion of the wave front impinging on this region accumulates a phase $2\pi(2\Delta/\lambda)$ relative to the datum (which is taken to be phase 0), after reflection from the micromirror via a double traversal of the distance Δ. For example, when reflected from a micromirror pulled back a distance $\Delta =$ 200 nm, light at $\lambda = 812$ nm, such as that in our experiment, accumulates a phase of approximately π radians.

We conducted experiments using three distinct phase distributions: (a) zero phase everywhere (flat mirrors); (b) a single line of micromirrors pulled down to implement a phase of π; and (c) two lines of micromirrors pulled down to implement a phase of π, separated by an undisturbed line of mirrors with phase 0. All three distributions are independent of one of the dimensions of the array, and are thus effectively one-dimensional distributions ($\mathbf{r} \rightarrow x$). This is helpful since it enables us to integrate along the uniform direction at D_1 and D_2.

The pump shown in Fig. 1 was the 406 nm line of a cw Kr-ion laser operated at a power of 30 mW. The nonlinear crystal was a 1.5-mm-thick BBO crystal cut for collinear (probe and reference emitted into the same beam), degenerate, type-I (probe and reference have the same polarization) SPDC. We chose a type-I collinear configuration, rather than a type-II (probe and reference with orthogonal polarizations) collinear configuration, such as that used in Refs. [8,9], or the type-I noncollinear configuration used in Ref. [4]. The advantage of the type-I collinear configuration is that the two down-converted beams are emitted in the same circularly symmetric spatial mode. This is useful for carrying out imaging experiments since artifacts arising from differences between the spatial distributions of the two beams, as well as peculiarities of beam shape, are eliminated. However, half of the photon-pair flux is lost in this configuration, as will be elaborated below.

The pump (extraordinary polarization) was separated from the down-converted photons (ordinary polarization) by means of a pair of Glan-Laser polarizing beam splitters (GL_1 and GL_2), placed before and after the nonlinear crystal, respectively. A long-pass colored glass filter (CGF) of cutoff wavelength 560 nm was used to further separate away the pump. The photon pairs were then permitted to impinge on a nonpolarizing beam splitter (BS). As a result, half of the pairs are separated into the two output beams, whereas the other half of the pairs emerge together at the same output port and thus fail to contribute to coincidences; this accounts for the 50% reduction of photon flux mentioned above.

The PROBE beam reflected from the beam splitter impinges on the phase object and is then reflected to a single-photon-detector module D_1 (fiber-coupled EG&G SPCM-AQR-15). The detector is preceded by a vertical slit P_1 of width 1.4 mm and an interference filter F_1 (centered at 800 nm with a bandwidth of 66 nm) to eliminate any remaining pump photons. The detected photons are integrated along the direction parallel to the slit. The REFERENCE beam transmitted through the beam splitter, which does not interact with the object, is directed to an identical detection unit D_2 (vertical slit P_2 and filter F_2). However this detector is mounted on a computer-controlled stage that permits scanning of the beam. The electrical pulses from the two detectors are sent to a coincidence circuit ($\otimes$) with a 2-nsec timing window.

The distance from the NLC, via reflection from the BS, to the micromirrors is $d_a = 1.17$ m; the distance from the micromirrors to detector D_1 is $d_b = 1.98$ m; the distance from the NLC, through the BS, to D_2 is $d_2 = 3.96$ m. For this configuration, the diffraction pattern is formed at a distance $d = d_2 + d_a = 5.13$ m from the mirrors; this is the distance from the mirrors to the BS to the NLC, then back to the BS and on to D_2. Since the width of the object is $a = 3.6$ mm, the diffraction Fresnel number is $N_F = (a/2)^2/\lambda d \approx 0.78$.

Results.—The results are displayed in Fig. 2 for the three phase objects on which we conducted imaging experiments. In each case, the coincidence counts measured by detectors D_1 and D_2 are plotted as a function of the scanned position x_2 of detector D_2. Though slightly wider, the theoretical predictions based on the approximate model (thick solid curves) are seen to match the experimental results (filled circles connected by thin lines). We have also recorded the single-photon counts collected from D_2, independently of the counts recorded from D_1. This measurement is, of course, completely independent of the object; it represents the far-field pattern of the reference beam and thus depends only on the physical parameters of the pump and nonlinear crystal. The first object has a uniform phase distribution, $\theta(x) = 0$, which represents a highly reflecting, uniform mirror of finite aperture. The coincidence profile shown in Fig. 2(a) is the diffraction pattern of the object aperture, which is approximately the Fourier transform of this object.

The second object has a phase distribution that takes the form of a single strip of phase π in a uniform background of phase 0. We call this object a *phase slit.* The measured coincidence image presented in Fig. 2(b) has a double-peaked profile that is the Fresnel transform (approximately the Fourier transform) of the object phase distribution. This profile is dramatically different from that associated with the usual *amplitude slit*, which has a single central peak and smaller side lobes.

The third object is a double-phase slit. The measured coincidence profile displayed in Fig. 2(c) is qualitatively similar to that for the single phase slit illustrated in Fig. 2(b), but has a wider and deeper dip, and also lower peak values. There are two reasons for this: (1) The diffraction pattern for the double-phase slit is more spread out, and since no photons are absorbed by the phase object, the height of the distribution must be lower.

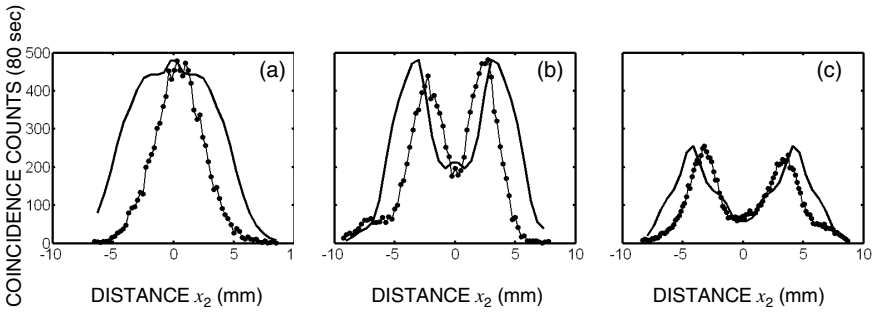

FIG. 2. Experimental coincidence counts (filled circles connected by thin lines) measured from D_1 and D_2 as the position x_2 of detector D_2 is scanned. The collection time is 80 sec per point. The thick solid curves are the theoretical predictions. (a) Object with uniform phase 0; (b) single-slit object with phase π; (c) double-slit object with phase π separated by a line of phase 0.

(2) The rate of single photons detected by D_1 is smaller. The pattern reflected towards D_1 is wider, and since the pinhole has the same size, fewer photons are collected for the double-phase slit, thereby resulting in a further reduction of coincidence counts for this case. We have recorded the single-photon rate at both detectors in the two cases. It is gratifying that the incorporation of this additional reduction factor into the theoretical calculation leads to a ratio of heights of the theoretical patterns that match experiment.

It is worth emphasizing that the diffraction profile of the double-phase-slit object is dramatically different from that of a conventional double-slit amplitude object; the latter exhibits a single central peak with smaller side lobes, rather than a double-peaked distribution. For the same configuration and dimensions, the amplitude object produces a substantially wider diffraction pattern. Note, however, that a ''double-strip'' amplitude object (an aperture that transmits light everywhere except at two parallel strips) has a diffraction pattern similar to that of a double-phase slit of the same dimensions, but it has far less visibility (it is well known in phase lithography that the maximum contrast produced by slit modulation is obtained for π-phase-shift slits).

Conclusion.—We have experimentally demonstrated that a coherent image of a reflective pure phase object may be obtained by using a spatially incoherent probe beam. The experiments were directed toward measurements of the Fresnel (approximately Fourier) transform of simple phase objects, but other coherent images may be similarly measured. This includes phase-contrast imaging, which may be realized by splitting the probe beam into two laterally displaced probe beams transmitted through the object. It also includes holography, which may be realized by splitting the probe beam into a reference and an object beam as in conventional holography [26].

This work was supported by the NSF Center for Subsurface Sensing and Imaging Systems (CenSSIS); by the Quantum Imaging (QUANTIM) Research Project funded by the Information Societies Technology (IST) Programme of the European Community; and by the David & Lucile Packard Foundation. We are grateful to T. G. Bifano and the Boston Micromachines Corporation for providing us with the MEMS micromirror array. We thank A. N. Vamivakas and J. Hofman for technical assistance.

*Current address: M.I.T. Research Laboratory of Electronics, Room 36-229, 77 Massachusetts Avenue, Cambridge, MA 02139-4307, USA
Electronic address: raddy@mit.edu
†URL: http://www.bu.edu/qil

[1] D. N. Klyshko, *Photons and Nonlinear Optics* (Nauka, Moscow, 1980), Chaps. 1 and 6, (translation published by Gordon and Breach, New York, 1988).
[2] A. Joobeur *et al.*, Phys. Rev. A **50**, 3349 (1994).
[3] P. H. S. Ribeiro *et al.*, Appl. Opt. **33**, 352 (1994).
[4] P. H. S. Ribeiro, S. Pádua, J. C. M. da Silva, and G. A. Barbosa, Phys. Rev. A **49**, 4176 (1994).
[5] G. A. Barbosa, Phys. Rev. A **54**, 4473 (1996).
[6] A. Joobeur *et al.*, Phys. Rev. A **53**, 4360 (1996).
[7] B. E. A. Saleh, A. Joobeur, and M. C. Teich, Phys. Rev. A **57**, 3991 (1998).
[8] T. B. Pittman *et al.*, Phys. Rev. A **52**, R3429 (1995).
[9] T. B. Pittman *et al.*, Phys. Rev. A **53**, 2804 (1996).
[10] A. F. Abouraddy *et al.*, Phys. Rev. Lett. **87**, 123602 (2001).
[11] A. F. Abouraddy *et al.*, J. Opt. Soc. Am. B **19**, 1174 (2002).
[12] R. S. Bennink *et al.*, Phys. Rev. Lett. **89**, 113601 (2002).
[13] A. Gatti *et al.*, Phys. Rev. Lett. **90**, 133603 (2003).
[14] E. Tan *et al.*, Eur. Phys. J. D **22**, 495 (2003).
[15] J. C. Howell *et al.*, quant-ph/0309122.
[16] R. Hanbury-Brown, *The Intensity Interferomenter* (Taylor & Francis, London, 1974).
[17] M. L. Goldberger *et al.*, Phys. Rev. **132**, 2764 (1963).
[18] B. E. A. Saleh *et al.*, Phys. Rev. A **62**, 043816 (2000).
[19] A. Gatti *et al.*, Phys. Rev. A **70**, 013802 (2004).
[20] D. Magatti *et al.*, quant-ph/0408021.
[21] W. Martienssen and E. Spiller, Am. J. Phys. **32**, 919 (1964).
[22] J. W. Goodman, *Introduction to Fourier Optics* (McGraw-Hill, New York, 1968).
[23] B. E. A. Saleh and M. C. Teich, *Fundamentals of Photonics* (Wiley, New York, 1991).
[24] D. V. Strekalov *et al.*, Phys. Rev. Lett. **74**, 3600 (1995).
[25] D. N. Klyshko, Usp. Fiz. Nauk **154**, 133 (1988) [Sov. Phys. Usp. **31**, 74 (1988)].
[26] A. F. Abouraddy *et al.*, Opt. Express **9**, 498 (2001).